ARCHIVES OF ELECTRICAL ENGINEERING VOL. X(Y), pp. 1-21 (2026)

Citation information: DOI 10.24425/aee.2026.2674

Research on demagnetization fault diagnosis of permanent magnet flux-switching linear motors based on few-shot learning

YONGLI LEI[1], LIWANG AI[2,3], XIAOZHUO XU[2,3*], YAZHAO GAO[2], WANYU WANG[2]

[1]*Zhongshan Inspection Branch for Guangdong Institute of Special Equipment Inspection and Research*
Zhongshan, China

[2]*School of Electrical Engineering and Automation, Henan Polytechnic University*
Jiaozuo, China

[3]*Henan International Joint Laboratory of Direct Drive and Control of Intelligent Equipment*
Jiaozuo, China
e-mail: xxz@hpu.edu.cn

Abstract: Aiming at the problems of few samples of local demagnetization faults and high difficulty in air-gap magnetic field detection for permanent magnet flux-switching linear motors (PMFSLMs), this paper adopts the primary backplate magnetic flux leakage signal of PMFSLMs to characterize demagnetization fault, which effectively avoids air-gap magnetic field detection. A few-shot learning method based on a Siamese convolutional neural network (CNN) is adopted to diagnose and identify the demagnetization faults in PMFSLMs. Firstly, a finite element model (FEM) of the PMFSLM is established to analyze the electromagnetic characteristics of the PMFSLM, so as to obtain the backplate magnetic flux leakage data under different demagnetization conditions. Then, a dual-channel dataset of backplate magnetic flux leakage signals is constructed and thus the signals of magnetic flux density difference are reconstructed under different demagnetization faults. Finally, a few-shot learning method based on a Siamese CNN is used to establish a classification model for identifying different demagnetization faults. The finite element simulation results

This paper has been accepted for publication in the AEE journal. This is the version, which has not been fully edited and content may change prior to final publication.
Citation information: DOI 10.24425/aee.2026.2674

show that the proposed method can accurately identify different demagnetization locations and demagnetization combinations of the PMFSLM, and exhibits high accuracy under limited-sample conditions.

Key words: convolutional neural network, demagnetization, few-shot learning, leakage flux density of backplate, permanent magnet flux-switching linear motors

1. Introduction

The permanent magnets (PMs) and armature windings of permanent magnet flux-switching linear motors (PMFSLMs) are both installed on the rotor primary, while its stator secondary is only composed of a slotted iron core, which has the advantages of high efficiency, high thrust density, and low cost. It has great potential for applications in vertical lifting, logistics transmission, rail transit and other fields [1], [3].

PMs are an important component, and their magnetic field distribution has a significant impact on operation performance of PMFSLMs, PMs are generally affected by factors such as temperature, aging, external magnetic fields, and mechanical effects, resulting in reversible or irreversible demagnetization [4]–[7]. Due to the unique structure of PMFSLMs, PMs are embedded in the primary teeth and are more susceptible to demagnetization risk due to the heating effect of the winding. Therefore, conducting research on PMs demagnetization faults in the PMFSLMs is of great significance to ensure the safety and stable operation of the equipment.

The research on the diagnosis of demagnetization faults in motors mainly includes three parts: signal acquisition of demagnetization faults, signal feature extraction of demagnetization faults, and identification of demagnetization faults using algorithms.

Demagnetization fault signals are typically acquired by monitoring motor conditions via invasive or non-invasive sensors, which provide vibration, current, and voltage data.

In terms of fault signal feature extraction, current, voltage, vibration, torque, and magnetic flux density signals are commonly used as fault signals. These signals are often combined with the fast Fourier transform, short-time Fourier transform, wavelet transform, empirical mode decomposition, and other methods to extract fault features, thereby mining fault information and realizing demagnetization fault diagnosis of PM motors [8–9]. Reference [10] proposes a method combining wavelet packet and sample entropy to reconstruct the stator current through wavelet packet, perform spectral analysis on the stator current, and diagnose the demagnetization fault in permanent magnet synchronous motors (PMSMs). Reference [11] proposes using the fast

This paper has been accepted for publication in the AEE journal. This is the version, which has not been fully edited and content may change prior to final publication.
Citation information: DOI 10.24425/aee.2026.2674

Fourier transform (FFT) to analyze stator current harmonics combined with zero-sequence current, or zero-sequence current combined with q-axis current, to diagnose PMs' demagnetization faults at different speeds. The signal extraction methods for the above fault diagnosis have been widely used in rotating motors and have achieved certain results. However, most of them reflect the magnetic field changes when the PMs lose magnetism through voltage, current, and vibration signals, which are easily affected by high-frequency noise interference and cause diagnostic errors. Reference [11] uses an air-gap magnetic density signal for fault diagnosis of the Permanent Magnet synchronous linear motor. The air-gap magnetic density signal is not easily affected by high-frequency noise interference and can reflect the fault characteristics well. But for the PMFSLM, its PMs and windings are both located on the rotor side, with a small air-gap. The installation space of the air-gap magnetic density sensor is limited, and the signal is not easy to obtain.

In the field of fault classification and recognition, deep learning has developed rapidly over the past decade and has received increasing attention from researchers, becoming a hot topic in the field of fault diagnosis. In traditional machine learning algorithms, a substantial amount of knowledge related to the engineering field is required, and the design of feature extraction methods is limited. However, the birth of deep learning effectively solves the shortcomings of machine learning, which is good at extracting advanced abstract features from raw data and has good generalization ability. Therefore, it is widely used in scientific research fields related to feature extraction. Reference [13] improved the convolutional neural network (CNN) by applying enhanced design principles for fault diagnosis of rolling bearings. [14] used a deep neural network for adaptive feature extraction of faults, and then added classifiers to the deep metric network and top-level feature output layer to classify and recognize faults, achieving high-precision diagnosis of bearing faults. [15] adopted a three-phase current as the fault feature and used a one-dimensional CNN to classify an inter-turn short-circuit fault, and PM demagnetization fault in the PMSM with high accuracy. The above literature is mainly based on large sample data to study the feasibility of deep learning methods in motor fault diagnosis applications. However, there is relatively little research on the applicability of deep learning methods in the context of small sample data. In practical applications, the real-time requirements of complex working conditions or online diagnosis make it impossible to obtain sufficient fault samples. Therefore, it is extremely necessary to develop fault diagnosis methods based on small sample data.

This article proposes a non-invasive method for obtaining fault data to diagnose the demagnetization problem of PMFSLMs. Without relying on complex signal processing

This paper has been accepted for publication in the AEE journal. This is the version, which has not been fully edited and content may change prior to final publication.
Citation information: DOI 10.24425/aee.2026.2674

techniques, the original signal of backplate leakage magnetic flux density and the reconstructed signal of magnetic flux density difference are used as signal inputs. A few-shot learning strategy based on a Siamese CNN is adopted to adaptively extract features from the two signals for fault diagnosis and classification. The simulation results show not only the effectiveness of this method, but also the higher diagnostic accuracy than a CNN when there are fewer samples.

2. Topological structure and working principle

2.1. Topological structure

This article takes the PMFSLM as the research object, a structural model shown in Fig. 1. The three main components of the PMFSLM primary are the iron core, PMs, and windings. A PM is inserted between every two teeth of the iron core. The magnetization direction of the PMs is along the direction of motor motion, and the magnetization direction of each adjacent two PMs is opposite. Each PM is surrounded by a concentrated coil. The secondary is only composed of a salient-pole iron core. Based on the parameters listed in Table 1, a simulation model is established to conduct fault analysis on its PMs. The following assumptions are made:

1) PMFSLM only exists in the X-Y two-dimensional magnetic field.
2) The current inside the conductor is uniformly distributed.
3) PM materials are isotropic and PMs have uniform magnetization.

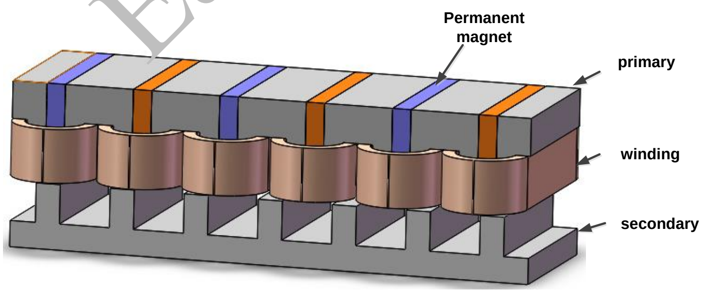

(a) PMFSLM 3D structure diagram

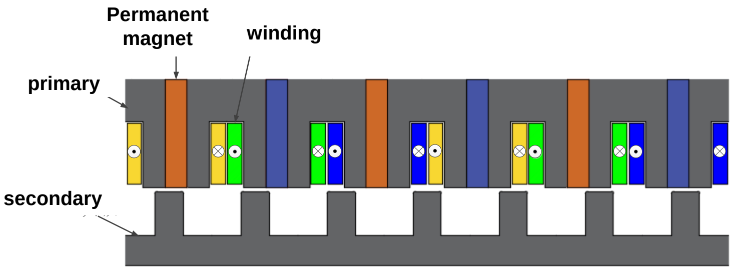

(b) PMFSLM sectional view

Fig. 1. Structure diagram of PMFSLM

Table 1. Main parameters of PMFSLM

Parameter	Value
PM material	N48H
Axial length/mm	120
PM width/mm	13
PM height/mm	66
Air-gap length/mm	2.5
Number of poles	6
Number of coil turns	179

2.2. Working principle

The operating principle of the PMFSLM follows the principle of minimizing the magnetic flux path, as shown in Fig. 2, which shows the relative positions of the primary and secondary at different times and the path of the PM flux linkage. At position 1, the armature winding flux linkage reaches a negative peak. When at the position shown in position 1, the winding flux linkage reaches its maximum value. At positions 2 and 4, the PM magnetic flux in the windings cancel each other out to zero. If the current is stopped, the motor will stop moving. If a current of right in and left out is applied to the winding in position 2, the primary iron core will generate an upward excitation magnetic flux, which will cause the primary to move to the left in position 3. The PM magnetic flux in the PMFSLM always exists. Moreover, as the position of the secondary teeth changes, the addition of excitation magnetic flux will continuously switch its path, thereby causing changes in the magnitude and direction of the magnetic flux in the primary winding and generating a back electromotive force.

This paper has been accepted for publication in the AEE journal. This is the version, which has not been fully edited and content may change prior to final publication.
Citation information: DOI 10.24425/aee.2026.2674

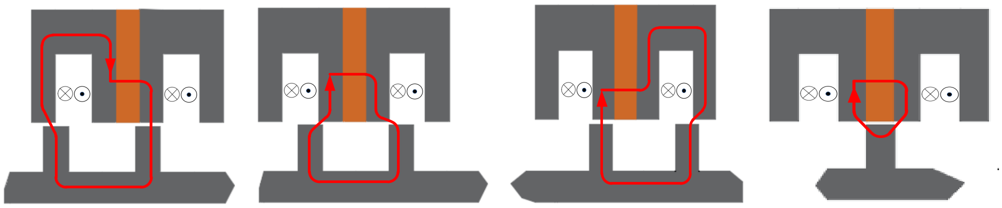

(a) position 1 (b) position 2 (c) position 3 (d) position 4

Fig. 2. Basic working principle of PMFSLM

3. Analysis of PMFSLM demagnetization faults

3.1. Finite element analysis of partial demagnetization in PMs

A 2D finite element model of the PMFSLM was established in a magnet to analyze the electromagnetic characteristics under healthy and demagnetized conditions [11].

The PM material used in the PMFSLM model is N48H. According to the B-H demagnetization curves of N48H, both the remanent flux density (B_r) and coercive force (H_c) are temperature-dependent. With the increase in temperature, B_r decreases slightly, while the absolute value of H_c decreases more evidently, indicating that the PM becomes more susceptible to irreversible demagnetization under high-temperature conditions. Similar finite-element-based demagnetization studies have evaluated the demagnetization behavior of permanent magnets in permanent magnet linear synchronous motors by tracking the operating points on the B-H curve under different current and temperature conditions [16]. In the finite element fault model of this study, the demagnetization degree was represented by reducing H_c of the selected PM. The variation of B_r was not independently considered.

The demagnetization ratio (D) was defined according to the reduction of H_c:

$$D = \frac{H_{c0} - H_{cd}}{H_{c0}} \times 100\%, \tag{1}$$

where H_{c0} is the coercive force of the healthy PM, and H_{cd} is the coercive force under the demagnetized condition. Thus, the coercive force under a given demagnetization ratio can be expressed as:

$$H_{cd} = (1 - D)H_{c0}. \tag{2}$$

This paper has been accepted for publication in the AEE journal. This is the version, which has not been fully edited and content may change prior to final publication.
Citation information: DOI 10.24425/aee.2026.2674

The demagnetized region was defined according to the considered fault type. In the finite element model, the selected PM region was assigned a reduced H_c value, while the remaining PMs retained their healthy magnetic properties. For combined demagnetization faults, the reduced H_c was applied simultaneously to the corresponding PM regions.

The finite element model was solved based on the magnetic vector potential formulation. The first-type and second-type boundary conditions were applied to the 2D solution domain. The model was discretized in the magnet, and the PM region, air-gap region, primary and secondary iron cores, as well as the backplate leakage flux density extraction path were included in the finite element calculation. From Fig. 3, it can be seen that when the PMFSLM experiences demagnetization failure, the magnetic field of the PM pole and the gap magnetic field, as well as the leakage magnetic field of the backplate, will be weakened to varying degrees. The validity of the model was checked by comparing the magnetic flux density distribution under healthy conditions with the working principle of the PMFSLM. The obtained magnetic field distribution was consistent with the expected flux-switching magnetic path, indicating that the model could be used for subsequent demagnetization fault analysis.

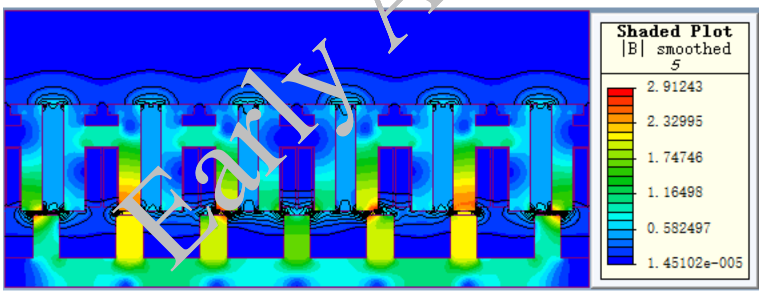

(a) normal state

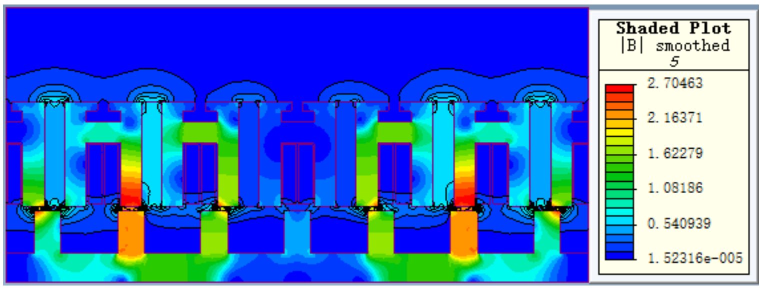

(b) Local demagnetization

Fig. 3. Flux distributions of PMFSLM

This paper has been accepted for publication in the AEE journal. This is the version, which has not been fully edited and content may change prior to final publication.
Citation information: DOI 10.24425/aee.2026.2674

3.2. Selection of fault characteristic quantities for PMFSLM

Due to its small air-gap length, the PMFSLM's air-gap magnetic density is difficult to extract. However, due to its unique structure, there is a certain amount of leakage magnetic phenomenon at the top of the PM, which can well reflect the fault characteristics when the PMs in the PMFSLMs demagnetize, and it is also easy to extract and measure. Therefore, this study uses the backplate leakage magnetic density as the fault signal to diagnose the fault in the PMFSLM. As shown in Fig. 4, the schematic diagram of PMFSLM backplate leakage magnetic flux density extraction is obtained uniformly along the red line at a constant speed. In daily production, high-precision Gaussian meters can be used to obtain the magnetic flux density of backplate leakage. The Gaussian meter probe is smoothly moved in the PMFSLM to obtain magnetic flux density data, which is recorded in the sampling PC and used to study the uniform demagnetization fault of the PMs in the PMFSLMs.

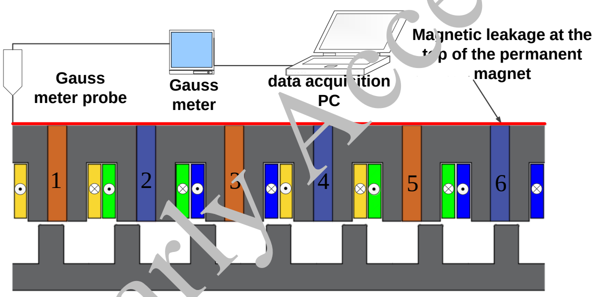

Fig. 4. Acquisition of magnetic flux leakage

3.3. PMFSLM demagnetization location and combination faults analysis

The PMFSLM used in this article is a three-phase PM linear motor. Due to the array relationship between the windings and the PMs, this study focuses on the first three PMs as one cycle, which has important reference value for the demagnetization situation of the later three PMs. Therefore, this article selects the first, second, and third PMs of the PMFSLM as the research objects. The PM was demagnetized by applying a reverse magnetic field, and then the leakage magnetic flux density of the backplate was determined.

Firstly, taking PM 3 as an example, different demagnetization degrees were applied to analyze the influence of severity variation on the backplate leakage flux density. As shown in Fig. 5, with the increase in demagnetization degree, the absolute value of the backplate leakage flux density decreases mainly in the region corresponding to PM 3. This indicates that the

This paper has been accepted for publication in the AEE journal. This is the version, which has not been fully edited and content may change prior to final publication.
Citation information: DOI 10.24425/aee.2026.2674

demagnetization degree mainly affects the local amplitude of the leakage flux density, while the position-related variation region remains basically consistent.

Therefore, this article will primarily focus on the identification of demagnetization locations and combinations. The fault type is classified based on the location and combination of the demagnetized PMs. Under this definition, samples with different demagnetization degrees of the same PM are regarded as intra-class variations within the same location category. This setting helps improve the robustness of the proposed method to changes in the severity of demagnetization, enabling it to effectively identify the location of the demagnetized PMs under different degrees of demagnetization.

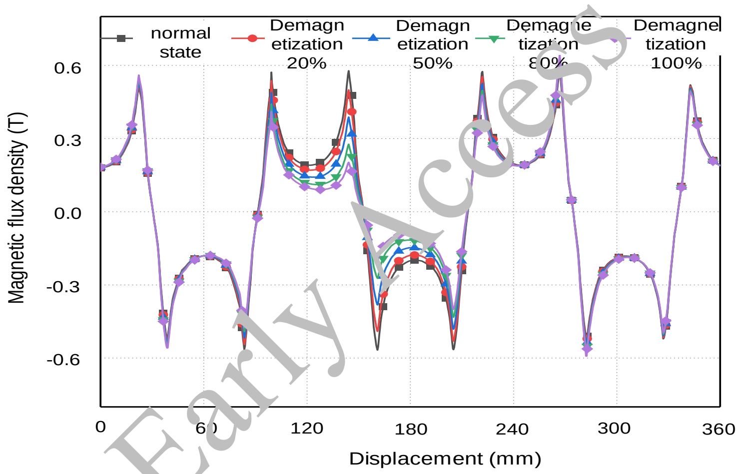

Fig. 5. Leakage flux density waveforms in different demagnetization state

Then, demagnetization analysis was conducted on PMs 1, 2, and 3, and the waveform of the backplate magnetic density was obtained as shown in Fig. 6. It can be seen that when PM 1 loses magnetism, there is a significant change in the amplitude of the backplate leakage magnetic density at 0–90 mm. When PM 2 loses magnetism, the amplitude of the backplate leakage magnetic density at 30–150 mm changes significantly. When PM 3 loses magnetism, the amplitude of the backplate leakage magnetic density at 90–210 mm changes significantly. The location of the magnetic density change is related to which specific PM loses magnetism, so different types of faults can be considered for different PM losses.

In summary, the demagnetization characteristics of PMFSLMs were analyzed by selecting PMs 1, 2, and 3. Therefore, the faults of the PMs were set in the form of combination, with a

This paper has been accepted for publication in the AEE journal. This is the version, which has not been fully edited and content may change prior to final publication.
Citation information: DOI 10.24425/aee.2026.2674

total of 7 fault arrangements corresponding to 7 types of faults. However, due to the idealization of simultaneous demagnetization of PMs 1, 2, and 3, only six types of faults were considered, as shown in Table 2.

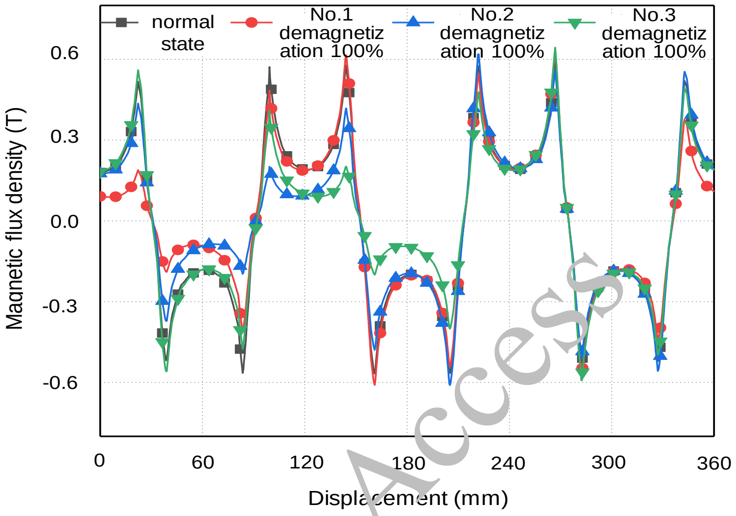

Fig. 6. Leakage flux density waveform when different PMs lose magnetism

Table 2. Partial demagnetization combination

Fault type number	Demagnetization type
1	No. 1 PM demagnetization
2	No. 2 PM demagnetization
3	No. 3 PM demagnetization
4	No. 1 and No. 2 PMs demagnetized simultaneously
5	No. 1 and No. 3 PMs demagnetized simultaneously
6	No. 2 and No. 3 PMs demagnetized simultaneously

Establish six demagnetization fault models in Table 2 through finite element simulation, then analyze these six demagnetization faults using 50% demagnetization of PMs. Figure 7 shows the magnetic flux density waveforms of the backplate leakage for the six types of demagnetization faults.

This paper has been accepted for publication in the AEE journal. This is the version, which has not been fully edited and content may change prior to final publication.
Citation information: DOI 10.24425/aee.2026.2674

From Fig. 7, it can be seen that different types of demagnetization faults not only have different amplitudes of backplate leakage magnetic flux density, but also have different positions of amplitude decrease. Therefore, the raw data of backplate leakage magnetic flux density can be used as signal input for few-shot learning.

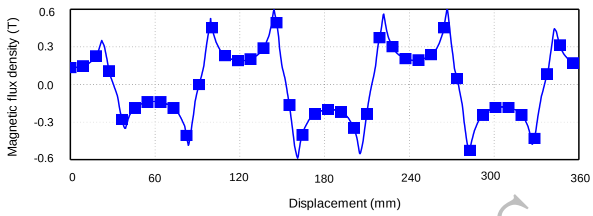

(a) Fault type 7.1

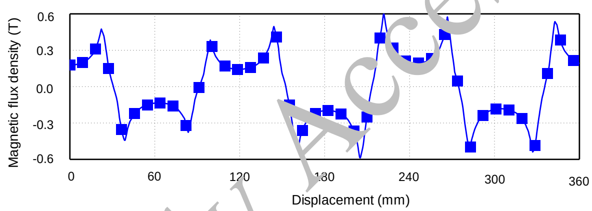

(b) Fault type 7.2

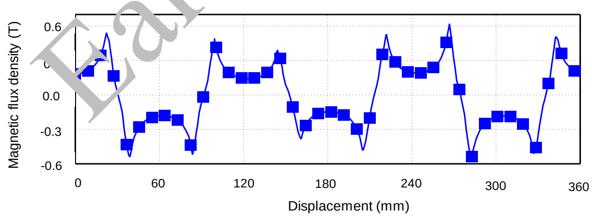

(c) Fault type 7.3

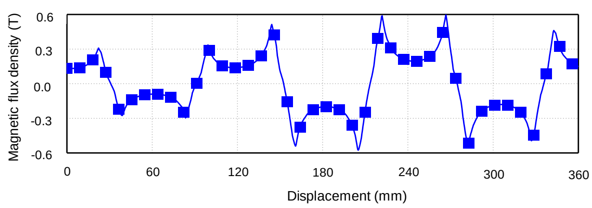

(d) Fault type 7.4

This paper has been accepted for publication in the AEE journal. This is the version, which has not been fully edited and content may change prior to final publication.
Citation information: DOI 10.24425/aee.2026.2674

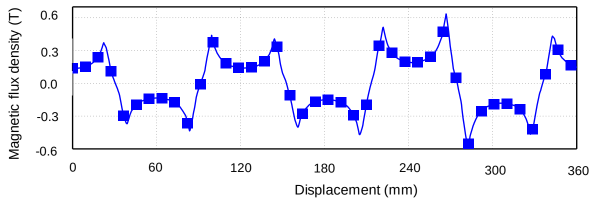

(e) Fault type 7.5

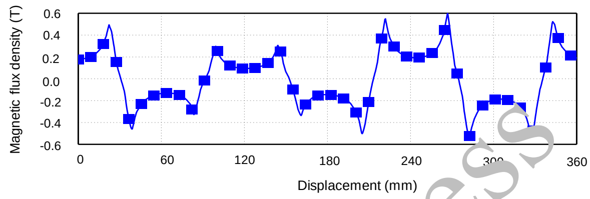

(f) Fault type 7.6

Fig. 7. Leakage flux density waveforms in different fault types

In order to ensure the accuracy of fault diagnosis, this study proposes a method for reconstructing the magnetic density difference, which involves reconstructing the fault based on the difference between the normal magnetic density and the fault magnetic density. This method can fuse the difference with the original data signal to serve as the signal input for few-shot learning. Figure 8 shows the waveform of the magnetic density difference for 6 fault types. It can be characterized not only by amplitudes, but also by waveform trends. Therefore, the reconstructed magnetic density difference waveform can be used as a signal input.

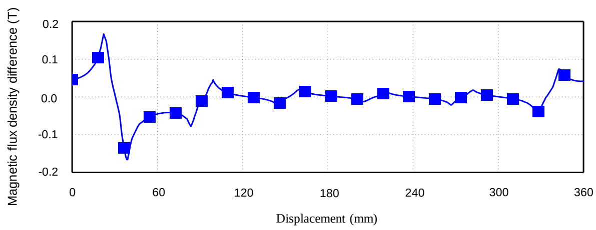

(a) Fault type 8.1

This paper has been accepted for publication in the AEE journal. This is the version, which has not been fully edited and content may change prior to final publication.
Citation information: DOI 10.24425/aee.2026.2674

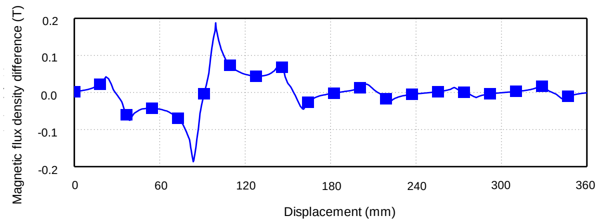

(b) Fault type 8.2

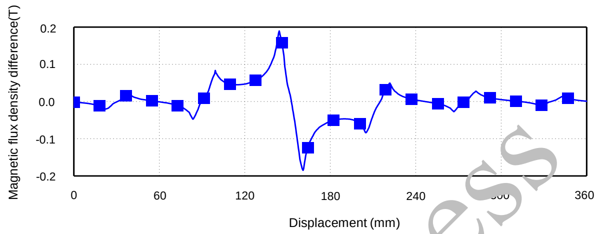

(c) Fault type 8.3

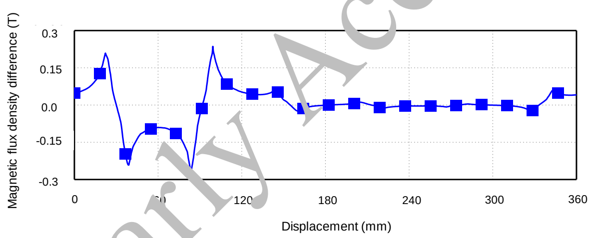

(d) Fault type 8.4

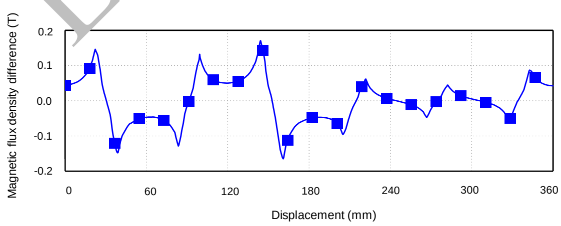

(e) Fault type 8.5

This paper has been accepted for publication in the AEE journal. This is the version, which has not been fully edited and content may change prior to final publication.
Citation information: DOI 10.24425/aee.2026.2674

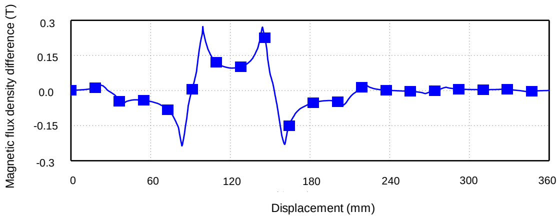

(f) Fault type 8.6

Fig. 8. Leakage flux density waveforms difference in different fault types

4. Demagnetization fault diagnosis

4.1. Few-shot learning model based on Siamese CNN

Few-shot learning is a training set with only a small number of labels used for related learning tasks. Firstly, it trains the model using a set of samples of the same or different categories (x_1^i, x_2^i). Its input is samples of the same or different categories, and its output is the probability that two input samples are the same $P(x_1^i, x_2^i)$. Unlike traditional classification, few-shot learning can be summarized as an *N*-shot *K*-way problem.

In one shot *K*-way testing, a support set S is given and a test sample $\bar{x}$ is classified, as shown in (3). The support set contains *K* samples, each with a feature label *y*.

$$S = \{(x_1, y_1), \ldots, (x_K, y_k)\}. \tag{3}$$

Then classify the test samples based on the support set, as shown in (4).

$$C(\bar{x}, S) = \underset{c}{\operatorname{argmax}}(P(\bar{x}, x_c)), \quad x_c \in S. \tag{4}$$

In the *N*-shot *K*-way test, the *N*-Shot *K*-way indicates that the support set contains *K* different categories, each with *N* labeled samples $(S_1, \ldots, S_N)$. Equation (5) is the classification function of the *N*-shot *K*-way model that determines which category of the support set the test sample should belong to.

$$C\left(\bar{x}, (S_1, \ldots, S_N)\right) = \underset{c}{\operatorname{argmax}}\left(\sum_{n=1}^{N} P\left(\bar{x}, x_{cn}\right)\right), \quad x_{cn} \in S_n. \tag{5}$$

The few-shot learning selected in this article is a diagnostic strategy based on a Siamese CNN. CNN, a foundational deep learning algorithm inspired by the mammalian visual system, is a

This paper has been accepted for publication in the AEE journal. This is the version, which has not been fully edited and content may change prior to final publication.
Citation information: DOI 10.24425/aee.2026.2674

feedforward network utilizing convolutional operations. It is renowned for its superior feature extraction capability and efficiency in processing spatially correlated, multi-channel information. Consequently, CNNs find broad applications in computer vision and speech recognition. A typical CNN architecture is composed of three primary types of layers: convolutional, pooling, and fully-connected layers. As shown in Fig. 9, a Siamese CNN structure model is used in this paper, which consists of two identical and weight-sharing CNNs connected by a similarity measurement layer to form a Siamese CNN model that can be used to measure sample similarity.

As shown in Table 3, the specific parameters of each layer of the Siamese CNN are presented. In order to obtain a larger perceptual field of view during feature extraction, a large-sized convolution kernel is first used for the first layer convolution to extract features. Then, a small convolution kernel is used for feature extraction, which can better extract fault features and is less susceptible to high-frequency noise interference in industrial environments, thereby improving the accuracy of fault diagnosis.

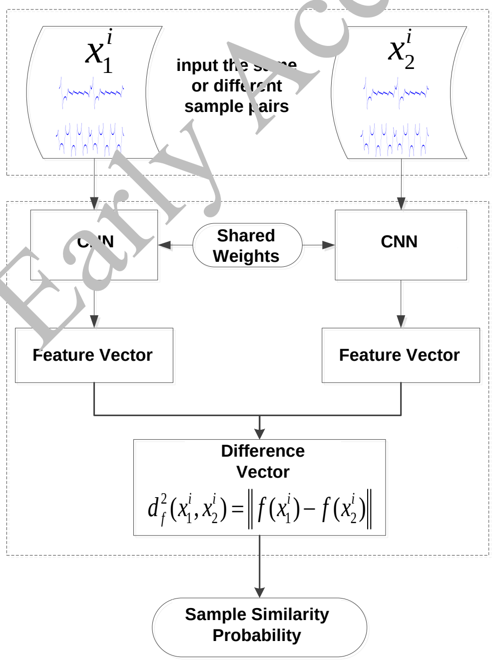

Fig. 9. Structure of Siamese CNN

Table 3. Main structural parameters of Siamese CNN

Network type	Key parameters
Convolution layer 1	Convolution kernel size 64, stride 16
Pooling layer 1	Pooling kernel size 2, stride 2
Convolution layer 2	Convolution kernel size 3, stride 1
Pooling layer 2	Pooling kernel size 2, stride 2
Convolution layer 3	Convolution kernel size 3, stride 1
Pooling layer 3	Pooling kernel size 2, stride 2
Convolution layer 4	Convolution kernel size 3, stride 1
Pooling layer 4	Pooling kernel size 2, stride 2
Convolution layer 5	Convolution kernel size 3, stride 1
Pooling layer 5	Pooling kernel size 2, stride 2
Fully connected layer	Number of neurons 100

Firstly, input the original sample data and the reconstructed difference data, and directly use the CNN to extract fault features from the data. Similarity comparison is performed using (6).

$$d_f^2(x_1^i, x_2^i) = \|f(x_1^i) - f(x_2^i)\|, \tag{6}$$

where d_f is the distance measurement formula between the samples, where f is the CNN network.

Output the similarity of Siamese CNN feature vectors to determine whether the output samples are similar. As shown in (7), P represents the probability that two input samples are the same.

$$P(x_1^i, x_2^i) = \mathrm{sigm}(FC(d_f^2(x_1^i, x_2^i))), \tag{7}$$

where sigm is the sigmoid function and FC is the dense fully connected layer.

The loss function is regularized cross entropy, as shown in (8). Let $t_j = y({x_1^i}_j, {x_2^i}_j)$ be a vector containing small batch labels, where j is the j-th sample pair of the i-th small batch. When ${x_1^i}_j$ and ${x_2^i}_j$ belong to the same fault category, then $t_j^i = 1$, if ${x_1^i}_j$ and ${x_2^i}_j$ do not belong to the same fault category, then $t_j^i = 0$.

$$L(x_1^i, x_2^i, t^i) = t^i \log(\, P(x_1^i, x_2^i)) + (1 - t^i) \log(\, 1 - P(x_1^i, x_2^i)) + \lambda^T |W|^2. \tag{8}$$

This paper has been accepted for publication in the AEE journal. This is the version, which has not been fully edited and content may change prior to final publication.
Citation information: DOI 10.24425/aee.2026.2674

Input a sample of the same or different categories, calculate the probability of two samples being similar using (7), and calculate the loss using (8). This article uses multiple one-shot K-way tests to simulate the N-shot K-way test. After the N-shot K-way test, N similar probabilities are obtained. The maximum probability sum of the same label is calculated using (5), and then fault classification is carried out.

4.2. Demagnetization location and combination classification result analysis

This article proposes a few-shot learning model for diagnosing PMFSLM faults. The dataset was generated from the finite element simulation results of six demagnetization location and combination faults. For each fault type, the original backplate leakage flux density signal and the reconstructed magnetic flux density difference signal were used as two input channels. The length of each channel was 120 000 data points, and each sample consisted of 1 024 consecutive data points. The test samples had the same length as the training samples and were generated without overlapping sampling. To evaluate the diagnostic performance of the proposed method under limited training samples, different numbers of training samples, including 90, 240, 420, 600, 1 200, and 2 400, were used for model evaluation. The diagnostic accuracy under different training-sample sizes was then compared with that of the conventional CNN model. As shown in Fig. 10, the diagnostic results with 2 400 training samples indicate that the few-shot learning strategy can effectively identify and classify different types of demagnetization faults in PMFSLMs, with an accuracy rate of 100%.

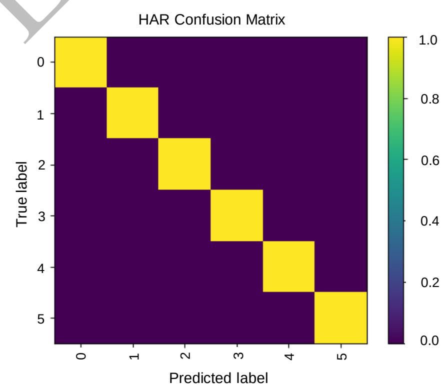

Fig. 10. Confusion matrix diagram of test result

This paper has been accepted for publication in the AEE journal. This is the version, which has not been fully edited and content may change prior to final publication.
Citation information: DOI 10.24425/aee.2026.2674

The comparison with the conventional CNN model is intended to specifically evaluate the contribution of the Siamese few-shot learning strategy under limited sample conditions. The conventional CNN was selected as the baseline because it has the same basic feature extraction mechanism as the proposed model, namely convolution-based feature learning from the input signals. Therefore, this comparison can more directly reveal whether the introduction of the Siamese structure and similarity metric learning improves the diagnostic performance when only a small number of fault samples are available.

Comparison was conducted with the classification results of the CNN algorithm when the training samples are 90, 240, 420, 600, 1 200, and 2 400. As shown in Fig. 11, when the number of training samples is small, the proposed Siamese CNN-based few-shot learning method achieves significantly higher accuracy than the conventional CNN. With the increase in training samples, the performance of both methods improves, and both reach 100% accuracy when sufficient training samples are available. This result indicates that the main advantage of the proposed method lies in its stronger generalization ability under limited-sample conditions. Therefore, the comparison with the conventional CNN is considered appropriate for verifying the main objective of this study, namely improving PMFSLM demagnetization fault diagnosis performance in small-sample scenarios.

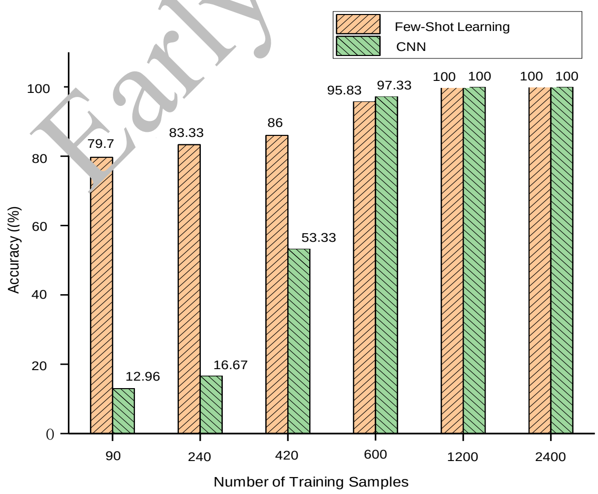

Fig. 11. Accuracy comparison for two fault classification method

This paper has been accepted for publication in the AEE journal. This is the version, which has not been fully edited and content may change prior to final publication.
Citation information: DOI 10.24425/aee.2026.2674

5. Conclusion

This article proposes a dual channel data reconstructed from the leakage magnetic flux density and magnetic flux density difference of the backplane as the fault signal. The few-shot learning strategy is adopted to identify PMFSLM demagnetization faults, and the following conclusions are drawn:

1) The backplate leakage flux density signal can effectively reflect the demagnetization fault characteristics of the PMFSLM. Compared with air-gap flux density measurement, it can be obtained outside the motor without installing a sensor inside the narrow air-gap region, which improves its practical measurement feasibility. Nevertheless, the signal may still be affected by sensor position, measurement noise, speed fluctuation, load variation, and temperature change under real operating conditions. However, since the present study is mainly based on FEM data, the influence of practical measurement errors and operating condition variations should be further investigated through experimental validation in future work.

2) The proposed Siamese CNN few-shot learning method can effectively identify different demagnetization locations and demagnetization combinations of PMFSLMs. The results show that the method achieves nearly 80% accuracy with only 90 training samples and reaches 100% accuracy when the number of training samples is 1 200.

3) A comparative study is conducted on the accuracy of few-shot learning and CNN diagnostic methods, and it is found that few-shot learning demonstrates a higher accuracy when the training samples are 90, 240, and 420. Future work will further investigate episode-based few-shot evaluation under multiple operating conditions, including 1-shot, 5-shot, and 10-shot settings with statistical confidence analysis.

Acknowledgements

This work is supported in part by the National Natural Science Foundation of China under Grant 52307050, the Key Research of Development and Promotion of Henan Province under Grant 252102241048, the Henan Provincial Natural Science Foundation under Grant 252300421328, the Outstanding Youth Fund of Henan Polytechnic University under Grant J2024-5, the Youth backbone Teacher Foundation of Henan Polytechnic University under Grant 2024XQG-01, and in part by the Innovative Team of Henan Polytechnic University under Grant T2023-2.

This paper has been accepted for publication in the AEE journal. This is the version, which has not been fully edited and content may change prior to final publication.
Citation information: DOI 10.24425/aee.2026.2674

References

[1] Thomas A.S., Zhu Z.Q., Jewell G.W., *Comparison of flux-switching and surface mounted PM generator for aerospace applications*, IET International Conference on Power Electronics, Brighton, UK, pp. 111–116 (2010), DOI: 10.1049/cp.2010.0060.

[2] Kayano S., Sanada M., Morimoto S., *Power characteristics of a PM flux switching generator for a low-speed wind turbine*, International Power Electronics Conference, Sapporo, Japan, pp. 258–263 (2010), DOI: 10.1109/IPEC.2010.5543884.

[3] Zhu Z.Q., Howe D., *Electrical machines and drives for electric hybrid and fuel cell vehicles*, Proceedings of the IEEE, vol. 95, no. 4, pp. 746–765 (2007), DOI: 10.1109/JPROC.2006.892482.

[4] Tang Xu, Wanf Xiuhe, Li Ying, Zhang Ran, *Demagnetization Study for Line-start PM Synchronous Motor During Starting Process*, Proceedings of the CSEE, vol. 35, no. 4, pp. 961–970 (2015), DOI: 10.13334/j.0258-8013.pcsee.2015.04.025.

[5] Xing Junqiang, Wang Fengxiang, Wang Tianyu, Zhang Yingbo, *Study on anti-demagnetization of magnet for high speed PM machine*, IEEE Transactions on Applied Superconductivity, vol. 20, no. 3, pp. 856–860 (2010), DOI: 10.1109/TASC.2009.2039121

[6] Lu Wei-fu, Zhao Hai-sen, Luo Ying-li, *Analysis of demagnetization field of line-start PM synchronous motor under abnormal operation conditions*, Electric Machines and Control, vol. 17, no. 7, pp. 7–14 (2013), DOI: 10.3969/j.issn.1007-449X.2013.07.002.

[7] Lu Weifu, Liu Mingji, Luo Yingli, Zhang Jian, *Demagnetization Field Analysis and Calculation for Line-start PM Synchronous Motor During Start Process*, Proceedings of the CSEE, vol. 31, no. 15, pp. 53–60 (2011), DOI: 10.13334/j.0258-8013.pcsee.2011.15.009.

[8] Ji Yongjian, Wang Hongjun, *A Revised Hilbert-Huang transform and its application to fault diagnosis in a rotor system*, Sensors, vol. 18, no. 12, 4329 (2018), DOI: 10.3390/s18124329.

[9] Yin Jintian, He Zhilong, Liu Li, Shao Wu, *Fault diagnosis method for PMSM demagnetization based on EMD and optimized SVM[J]*, Agricultural Equipment & Vehicle Engineering, vol. 11, pp. 123−128 (2024), DOI: 10.3969/j.issn.1673-3142.2024.11.022.

[10] Zhang Zhi-Yan, Ma Hong-Zhong, Yang Cun-Xiang, Sun Jun-Man, *Demagnetization fault diagnosis in PM synchronous motor combination wavelet packet with sample entropy*, Electric Machines and Control, vol. 19, no. 2, pp. 26–32 (2018), DOI: 10.15938/j.emc.2015.02.005.

[11] Rosero J., Cusido J., Garcia A., Ortega J.A., Romeral L., *Study on the PM demagnetization fault in PM synchronous machines*, The 32nd Annual Conference of the IEEE Industrial Electronics Society, Paris, France, pp. 1269–1274 (2006), DOI: 10.1109/IECON.2006.347598.

[12] Zhang Dan, Zhao Jiwen, Dong Fei, Song Juncai, Dou Shaokun, Wang Hui, Xie Fang, *Partial Demagnetization Fault Diagnosis Research of PM Synchronous Motors Based on the PNN Algorithm*, Proceedings of the CSEE, vol. 39, no. 1, pp. 26–32 (2019), DOI:10.13334/j.0258-8013.pcsee.172531.

[13] Zhou Chen-Lin, Dong Shao-Jing, Li Ling, Tang Bao-Ping, He Kun, Mu Shu-Feng, Zhang Xiao-Ting, *Method to improve convolutional neural network in rolling bearing fault diagnosis with multi-state feature information*, Journal of Vibration Engineering, vol. 33, no. 4, pp. 854–860 (2020), DOI: 10.16385/j.cnki.issn.1004-4523.2020.04.024.

[14] Li Xiaojuan, Xu Zengbing, Xiong Wen, Wang Zhigang, Tan Junjie, *Bearing fault diagnosis method based on deep metric learning*, Journal of Vibration and Shock, vol. 39, no. 15, pp. 25−31 (2020), DOI: 10.13465/j.cnki.jvs.2020.15.004.

[15] Ma Li-Ling, Liu Xiao-Ran, Shen Wei, Wang Junzheng, *Motor Fault Diagnosis Method Based on an Improved One-Dimensional Convolutional Neural Network*, Transactions of Beijing Institute of Technology, vol. 40, no. 10, pp. 1088–1093 (2020), DOI: 10.15918/j.tbit1001-0645.2019.201.

[16] Yücel E., Cunkas M., Knypiński Ł., *Evaluation of Magnet Demagnetization Behavior in Permanent Magnet Linear Synchronous Motors[J]*, Electrical Engineering and Energy, pp. 52–63 (2025), DOI: 10.64470/elene.2025.1005.